

AN EDGE-FEATURE-DESCRIPTION-BASED SCHEME COMBINED WITH SUPPORT VECTOR MACHINES FOR THE DETECTION OF VORTEX-INDUCED VIBRATION

TSUN-KUO LIN

Department of Information Technology and Communication
Shih Chien University
No. 200, University Road, Neimen, Kaohsiung 84550, Taiwan
tklin@mail.kh.usc.edu.tw

Received September 2017; revised January 2018

ABSTRACT. *Vortex-induced vibration (VIV) has been studied over the past decades because vibration may cause serious damages to structures such as bridges, pipelines, skyscrapers, and airplanes. Detecting VIV has long been a challenge. For example, when attempting to detect VIV, inspectors might fail to use multiple hot-wire or hot-film probes during concurrently measurement of the whole flow field. This study proposes a novel vision-based method for detecting the wake patterns of VIV; it employs an edge-feature-description (EFD)-based scheme with a multiclassifier of support vector machines (SVMs). The proposed hybrid EFD/SVM method detects and adaptively segments wake-pattern images for effective classification of the patterns. The VIV can be detected on the basis of the classification results. The experimental results demonstrated that the proposed method can effectively detect the VIV using a vision-based algorithm, which incorporates hybrid EFD/SVM for classifying wake-pattern images. The method applies a nondestructive scheme for detecting the VIV and achieves high recognition rates when classifying the wake patterns of VIV.*

Keywords: Edge feature description, Hybrid vision-based method, Support vector machines, Vortex-induced vibration

1. Introduction. The flow of fluids around structures is often found in a variety of engineering equipment, ranging from marine structures, such as marine risers and tension-leg-platform cables, to units used in various power generation plants and chemical plants, such as tube bundles in boilers and heat exchangers. Vortex-induced vibration (VIV) may occur and cause serious damage to such structure when the asymmetric vortices are shed from the structure and the vortex shedding frequency matches the structure's natural frequency. Therefore, understanding VIV, and detecting it, have become higher priorities because designers are using materials to their limits, delivering structures that are progressively lighter and more flexible, and thus, more prone to vibration.

The VIV of a flexible circular cylinder or tube subjected to cross flow has been investigated. For the dynamic response from the VIV, Huera-Huarte et al. [1] presented towing tank experiments on the VIV of low mass ratio long flexible cylinders. Feng et al. [2] investigated the nonlinear dynamic behaviors and the characteristics of the response of a three-dimensional flexible tube to VIV. Recently, flow control methods have been employed to suppress asymmetric vortices and VIV. Tang et al. [3] used synthetic jet actuator arrays for controlling flow separation. Wang et al. [4] presented active control of the wakes and the VIV of a single circular cylinder using a pair of synthetic jets at a low Reynolds number. Park et al. [5] employed localized surface roughness to suppress the VIV of an elastically mounted circular cylinder. Existing methods that have been

proposed to suppress VIV using flow control include active [3,4] and passive [5] schemes. However, effective detection of VIV has not been solved so far. Serious damages to numerous structures could be avoided if VIV could be reliably detected in advance. Poor measurements of the flow field are common causes of poor performance in VIV detection. Employing multiple hot-wire/hot-film probes for concurrently measuring the whole flow field has long been a challenge. Therefore, the current study proposes a vision-based technique that uses a nondestructive scheme to detect VIV. The proposed method effectively employs hybrid EFD/SVM to classify the wake patterns of vibrations and to detect VIV on the basis of the classification results.

Based on previous studies, SVM-based methods can be used in the work. In this study, we propose an EFD-based scheme with a multiclassifier of SVMs for the VIV detection. The contributions of this study are summarized as follows. The method employs a hybrid vision-based strategy incorporating SVM results for nondestructive detection of object samples. The hybrid method can adaptively segment and effectively classify the samples. Finally, the detection system applies a hybrid EFD/SVM algorithm to solving the VIV detection problem encountered when using multiple hot-wire/hot-film probes for concurrently measuring the whole flow field. The remainder of this paper is organized as follows. Section 2 reviews related work. Section 3 presents the VIV detection system and the proposed method for classifying the samples. Section 4 presents the experimental results derived from applying the proposed algorithm to various samples, and a comparison of various existing methods. The final section offers the conclusions of this study.

2. Related Work. This section describes previous methods (including SVM applications) related to the proposed method, and finally addresses the differences between the proposed method and the previous approaches.

Recent studies have investigated SVM-based methods in machine learning and computer vision. Researchers have tried to solve detection problems using various SVM-based learning approaches. Yang and Su [6] used SVMs for automated diagnosis of sewer pipe defects and showed that SVMs outperformed a Bayesian classifier. Serdio et al. [7] utilized a fuzzy learning system with SVMs to operate in a completely unsupervised manner for fault detection. Tseng et al. [8] developed a classification model, based on the tuning of the parameters in different SVM kernels, to predict the outcome of a quality control process. Instrumentation associated with SVMs has been proposed as highly effective for classifying samples. Guillermo et al. [9] proposed a technique using SVMs operating on the power spectrum density of signals to identify noise and types of partial discharges. Barbosa et al. [10] demonstrated that the use of quadrupole inductively coupled plasma mass spectrometry associated with SVM was possible to predict the authenticity of organic rice samples. Liang et al. [11] proposed a multi-task ranking SVM model to simultaneously segment multiple images and demonstrated that the proposed approach outperformed the existing techniques. Hybrid feature extraction and SVM classifier were also investigated in computer vision. Yu et al. [12] proposed a method for multifocus image fusion using hybrid dual-tree complex wavelet transform and SVMs. They showed that their method outperformed previous methods in terms of visual quality and objective evaluation. Ebrahimi et al. [13] proposed SVM method with different kernel functions for classification of parasites and detection of thrips. They demonstrated that incorporation of the image processing technique with SVM method and choice of suitable region and color index was successful in detecting the target with an error less than 2.5%. Lekdioui et al. [14] presented a facial decomposition method based on texture/shape descriptors with SVM classifier for expression recognition and reached recognition rates more than 92%.

These published SVM-based methods are similar to the proposed SVM-based method. However, this study employed an EFD-based scheme combined with SVMs for effective object detection. This hybrid method uses a vision-based algorithm, which can adaptively segment images and effectively classify their patterns; this can be used to solve the VIV detection problem inherent to concurrent measurement of a whole flow field with multiple hot-wire/hot-film probes. The present study quantitatively compared existing methods in VIV detection.

3. Proposed Method. A water tunnel was designed and built for this study. The VIV of a cylinder was conducted in the closed loop water tunnel. Water flow was driven through this tunnel by a variable speed pump. After passing through a filter, the water entered a diffuser, which provided a gradual transition from 0.1 m diameter circular pipe to a rectangular channel of 0.6 m \times 0.6 m. A layer of honeycomb wire and several screens were installed in the rectangular channel to reduce turbulence. At the entrance of the test section, a pitot tube was used to monitor the inlet flow velocity. A downstream transition region allowed water to exit the test section and flow into the storage tank. To obtain image signals, a fluorescent dye was added to the water and the industrial computer triggered a charge-coupled device (CCD) camera through Wi-Fi to acquire synchronous images. The synchronous image information was transmitted from the CCD camera to the industrial computer, which was equipped with a frame grabber for capturing the synchronous images.

Figure 1 displays a schematic of the VIV detection system. The proposed system enables sensing and classifying the wake patterns by employing a suitable processing (segmentation and classification) strategy on the basis of the sensing results. The system procedure can be summarized as follows: (1) input the wake-pattern images from the image queue; (2) execute the EFD-based algorithm [including an adaptive region-growing (ARG) segmentation and EFD-based extraction]; (3) classify patterns using SVMs; (4) confirm that no image remains in the image queue. Table 1 presents the classes of wake-pattern samples; 200 samples for each class were used for VIV detection. The EFD-based algorithm and the SVM adaptively selected suitable threshold T_p and edge descriptors C_i values for effective inspection of the wake patterns. Based on the selection, for inspecting the 200 class D synchronous images, the optimal threshold T_p and edge descriptors C_i were set to 0.52 and $\{C_4, C_5, C_6, C_7\}$, respectively; T_p and C_i were obtained from the

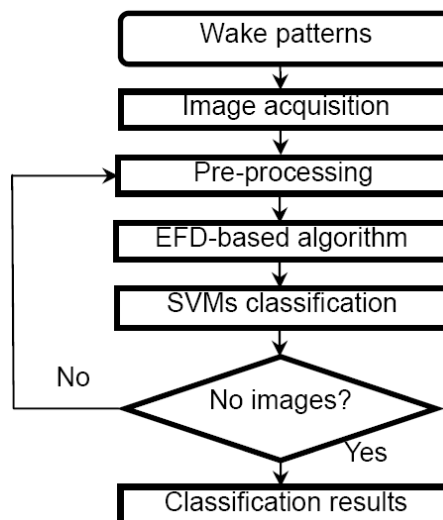


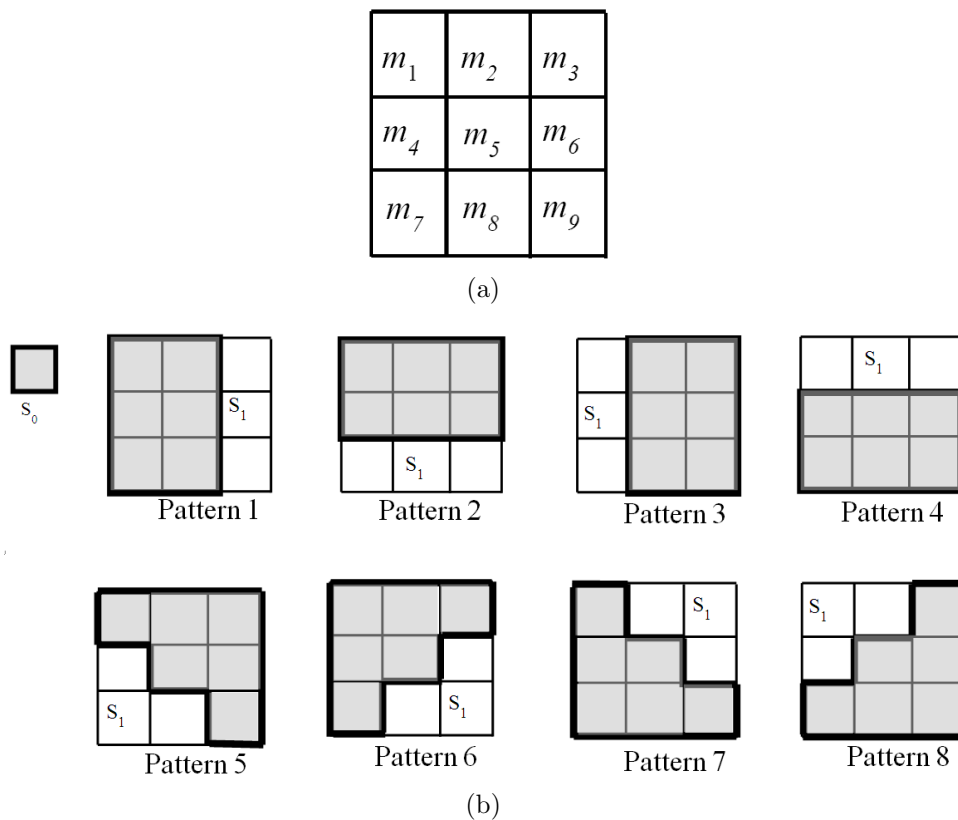
FIGURE 1. Schematic of the proposed VIV detection system

TABLE 1. Classes of the wake-pattern samples used in the experiments

Inlet flow velocity	Class
0.90 m/s	A
1.30 m/s	B
1.40 m/s	C
1.75 m/s	D

hybrid EFD/SVM method for the class D samples. The input images were converted to 1024×768 pixel images with an 8-bit gray level. The 256 gray levels were normalized to values within the range from 0 to 1. The hybrid EFD/SVM processing included an EFD-based algorithm and an SVM classification. The procedure for the EFD/SVM processing can be summarized as follows: (1) the EFD-based algorithm extracted features as edge descriptors from the input images; (2) the SVM automatically selected the thresholds for the descriptors; (3) the most suitable threshold and descriptors were obtained from among several descriptors. The procedure was complete for a given sample when no image remained in the image queue. T_p and C_i were reset and other samples were inspected similarly. The inspection was complete for all samples when the image queue was empty.

The EFD-based algorithm includes ARG segmentation [15] and EFD-based extraction. The EFD-based extraction employs an edge feature description for the ARG segmented image. According to the 3×3 mask depicted in Figure 2(a), edge pixels in the segmented images typically belong to one of eight possible edge patterns [Figure 2(b)]. In the edge pattern, nine pixels can be divided into two separate groups, namely S_0 and S_1 . For Edge Patterns 1-4, feature vector $x = (d_1, d_2, d_3)$, where $d_1 = m_1 + m_4 + m_7$ and $d_2 =$

FIGURE 2. (a) 3×3 mask and (b) patterns 1-8

$m_2 + m_5 + m_8$, $d_3 = m_3 + m_6 + m_9$, is used for edge description. For Edge Patterns 5-8, two feature vectors x and $y = (d_4, d_5, d_6)$, where $d_4 = m_1 + m_2 + m_3$, $d_5 = m_4 + m_5 + m_6$ and $d_6 = m_7 + m_8 + m_9$, are used for edge description. A value of 1 is set for initial seeds in the ARG segmentation. The values of the pixels in S_0 and S_1 are 1 and 0, respectively. Therefore, the procedures of this method are summarized as follows. (1) Calculate x in a segmented image. (2) Record x if x is $(3, 3, 0)$, $(2, 2, 2)$, or $(0, 3, 3)$. (3) Record x and calculate y if x is $(1, 2, 3)$ or $(3, 2, 1)$. (4) Record y if y is $(1, 2, 3)$ or $(3, 2, 1)$. After all pixels in an image have been processed using the aforementioned procedure, the edge is classified using feature vectors x and y . The edge descriptor E from the feature description is expressed as

$$E = \{C_i\}, \quad i = 1, 2, \dots, 7 \quad (1)$$

where C_i represents the seven coefficients of the normalized edge numbers from Edge Patterns 1, 2(4), 3, 5, 6, 7, and 8, and C_i ranges from 0 to 1.

The hybrid EFD/SVM method was proposed for adaptively selection of suitable T_p and C_i values for effective inspection of the wake patterns. Consider the set of feature values belonging to two separate classes $(x_1, y_1), \dots, (x_N, y_N)$ with input $x_i \in R^N$ (N -dimensional input space) and class labels (target output) $y_i \in \{1, -1\}$. An SVM was employed to implement the wake-pattern classification. An SVM constructs a hyperplane as a decision surface to maximize the margin of separation between positive and negative examples [16]. The conventional SVM is a tool for solving two-class problems. The common approaches for applying it to a multiclass problem involve converting the multiclass problem into several binary-class problems. The SVM algorithm requires only $N - 1$ SVMs for an N -class problem, which reduces the computation time during inspection. The SVMs are SVM 1, SVM 2, and SVM 3; each SVM is trained to function differently. SVM 1 divides all pattern samples into two classes, $\{A, B\}$ and $\{C, D\}$; SVM 2 and SVM 3 divide $\{A, B\}$ and $\{C, D\}$ into $\{A\}$, $\{B\}$, $\{C\}$, and $\{D\}$. The SVMs continue until all the samples have been identified, after which the classification is stopped. For SVM classifiers, the parameter C and the Gaussian radial basis function (RBF) kernel parameter γ must be optimized. High testing accuracy was realized when $C = 2^{13}$ and $\gamma = 2^{-7}$ were used in the SVMs. Table 2 lists the classification results for different sample sizes, indicating that sample sizes of 280, 400, and 600 in each test class are apparently unrelated to the classification results.

TABLE 2. Classification results using different sample sizes for each class

Sample size	Training	Validation	Accuracy rates (%)
70	20	50	83
80	30	50	89
140	40	100	91
280	80	200	96
400	100	300	96
600	200	400	96

As shown in Figure 3, the hybrid EFD/SVM algorithm applies the following steps to adaptively obtaining T_p and C_i for the wake-pattern inspection.

Step 1: A total of 200 sample images are tested for a given number of descriptors $\{C_i\}$, $i = 1, 2, \dots, 7$.

Step 2: Given a value of 1 for initial seeds in the gray-level image, the threshold values T_i are set in the range 0.01-0.99 sequentially; $\{T_i\} = \{0.01, 0.02, 0.03, \dots, 0.99\}$, $i = 0, 1, 2, \dots, 98$.

Step 3: The ARG segmentation is implemented using a set of initial seeds and groups neighboring pixels with each initial seed within the growth regions on the basis of $\{T_i\}$ [15].

Step 4: EFD-based extraction is implemented on the basis of a given number of descriptors and extract features as edge descriptors $\{C_i\}$ from the segmented image.

Step 5: The SVMs classify the edge descriptors on the basis of $\{T_i\}$ and obtain the classification results.

Step 6: The recognition rate is determined at each adjustable threshold T_i for the given image.

The recognition rate is defined as follows:

$$\text{Accuracy} = \left(\frac{N_C}{N} \right) \times 100\% \quad (2)$$

where N_C is the number of accurately classified images in the test run, and N is the total number of test sets (N is 200 in this case). If the recognition rate exceeds a given value δ , then Step 7 commences; otherwise, Steps 2-6 are repeated.

Step 7: The process stops when the sample images in all cases of the given number of descriptors $\{C_i\}$ have been tested; otherwise, Steps 1-6 are repeated. In addition, the algorithm stops when any T_i fails to satisfy the condition in Step 6.

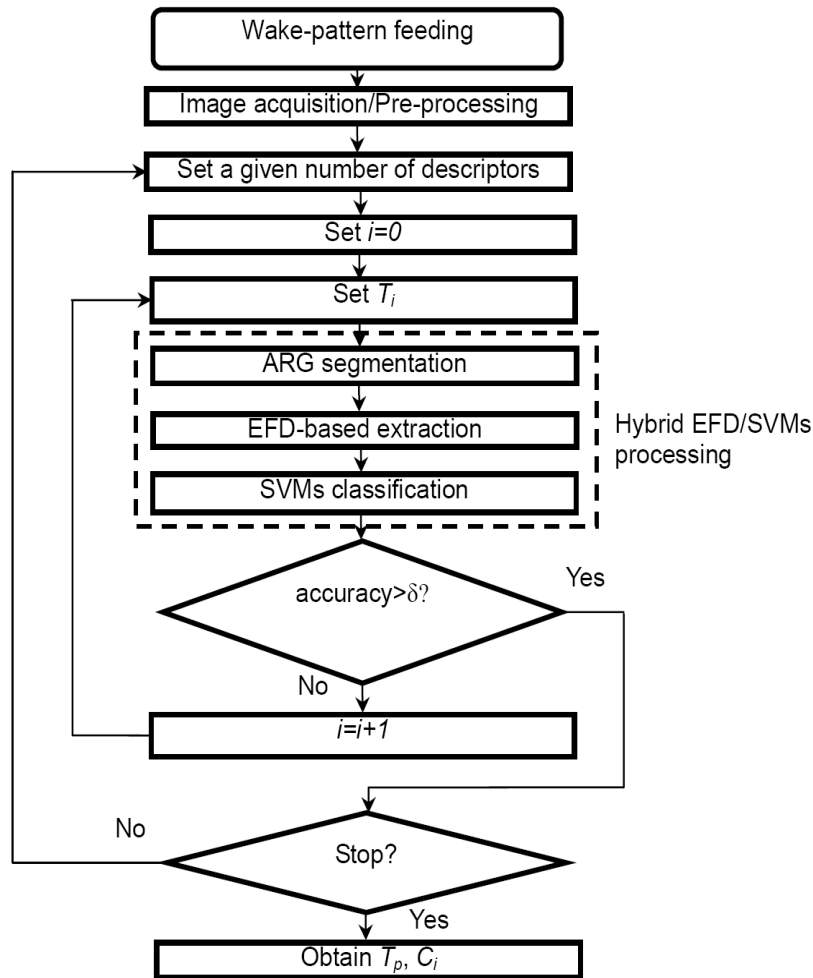


FIGURE 3. Flow diagram of the EFD/SVM algorithm

Suppose, for example, that Step 1 tests some set of sample images with descriptors C_4 , C_5 , C_6 , and C_7 . Step 2 sequentially sets T_i in the range 0.01-0.99. Step 3 implements the ARG segmentation. Step 4 extracts the edge features. Step 5 then classifies the edge features using the SVMs. When the given value δ is 0.9 (i.e., 90% accuracy rate), the process repeats Steps 2-6 until T_i exceeds 0.75. Step 7 then stops the process for the C_4 , C_5 , C_6 , and C_7 cases. In this test, the algorithm adaptively obtained suitable T_p and C_i as 0.76 and $\{C_4, C_5, C_6, C_7\}$, respectively.

4. Experimental Results. First, the study employed a general classification to test the EFD/SVM algorithm. Table 3 presents the wrench samples used for the general classification. The edge descriptors (E_1 , E_2 , and E_3) of the wrench samples are listed in Table 4. The E_1 , E_2 , and E_3 were normalized as $\{0.03, 0.22, 0.03, 0.32, 0.80, 0.40, 1\}$, $\{0.04, 0.24, 0.03, 0.25, 0.86, 0.28, 1\}$, and $\{0.04, 0.26, 0.04, 0.26, 1, 0.10, 0.94\}$, respectively. For the test case, 80 wrench images were randomly selected as training samples, and 200 wrench images were used for the classification. Table 5 lists the classification results obtained using the EFD/SVMs algorithm and demonstrates an average accuracy rate of 96%.

TABLE 3. Classes of wrench samples used for a general classification

Specification	Class
305 mm (12")	E
254 mm (10")	F
203 mm (8")	G

TABLE 4. Numbers of edges (1-8) in the descriptors E_1 , E_2 , and E_3 for the corresponding classes E, F, and G, respectively

Descriptor\Edge	1	2(4)	3	5	6	7	8
E_1	503	3428	442	4987	12475	6243	15598
E_2	463	2898	401	3092	10549	3458	12222
E_3	414	2551	353	2573	9953	1012	9342

TABLE 5. Test results using the EFD/SVM algorithm for a general classification, T (rows): true values, P (columns): predicted values

T\P	E	F	G
E	192	5	3
F	4	191	5
G	3	4	193

Then, the experiment was conducted to test the accuracy of the proposed algorithm for VIV detection. As listed in Table 2, 80 sample images were randomly selected as training samples, and 200 images without any flow and structural information were used for the classification. Figure 4 displays the segmentation results for class D with the given descriptors $\{C_i\} = \{C_6, C_7\}$, $\{C_4, C_5, C_6, C_7\}$. The segmented images obtained using the proposed algorithm with the given descriptors $\{C_4, C_5, C_6, C_7\}$ produced details and continuous contours for the wake patterns [Figure 4(b)]. Table 6 lists the classification results obtained using the proposed algorithm and demonstrates an average accuracy



FIGURE 4. Segmentation results for class D with a given number of descriptors using the EFD/SVM algorithm: (a) $\{C_6, C_7\}$ and (b) $\{C_4, C_5, C_6, C_7\}$

TABLE 6. Classification results using the EFD/SVM algorithm for the wake-pattern classes, T (rows): true values, P (columns): predicted values

T\P	A	B	C	D
A	192	4	4	0
B	1	191	6	2
C	0	6	192	2
D	0	3	4	193

TABLE 7. Example of the selection thresholds of samples with a given number of descriptors $\{C_i\}$

C_i	A	B	C	D	Accuracy rates (%)
C_6	0.81	0.75	0.61	0.50	72
C_6, C_7	0.82	0.74	0.60	0.51	79
C_5, C_6, C_7	0.80	0.75	0.61	0.52	87
C_4, C_5, C_6	0.81	0.76	0.62	0.53	91
C_3, C_5, C_6, C_7	0.80	0.77	0.63	0.51	92
C_4, C_5, C_6, C_7	0.83	0.76	0.62	0.52	96
C_3, C_4, C_5, C_6	0.82	0.77	0.62	0.53	93

rate of 96%. Table 7 illustrates the selection thresholds of the sample images with a given number of descriptors $\{C_i\}$. The thresholds for the descriptors were selected automatically by the SVMs. The most suitable descriptors $\{C_4, C_5, C_6, C_7\}$ were obtained from among several descriptors. This study employed the leave-one-out cross-validation (LOO-CV) with various thresholds to verify the selection threshold of the proposed algorithm. Table 8 shows that classes A, B, C, and D had the lowest mean squared errors (MSEs): 0.1365, 0.1075, 0.1238, and 0.1148, respectively. The threshold $T_i = 0.80, 0.75, 0.60,$ and 0.50 were the optimal selections for class A, B, C, and D in the detection because these values yielded the highest accuracy rate (Table 7).

The VIV detection was validated by measuring the dynamic response of the cylinder. The cylinder was equipped with two accelerators, both of which had sensitivity of 4.693 mV/g and a frequency response in the range from 2 to 8 kHz. The accelerometers were

TABLE 8. LOO-CV MSE of the descriptor C_6 with $T_i = 0.85, 0.80, 0.75, 0.70, 0.65, 0.60, 0.55,$ and 0.50 for the sample images

T_i	A	B	C	D
0.85	0.2827	0.3146	0.5067	0.5371
0.80	0.1365	0.2589	0.4462	0.4965
0.75	0.3344	0.1075	0.3978	0.4293
0.70	0.3729	0.2285	0.3354	0.3341
0.65	0.4025	0.3364	0.2473	0.2873
0.60	0.4381	0.3892	0.1238	0.2449
0.55	0.4720	0.4253	0.3062	0.1957
0.50	0.5173	0.4816	0.3643	0.1148

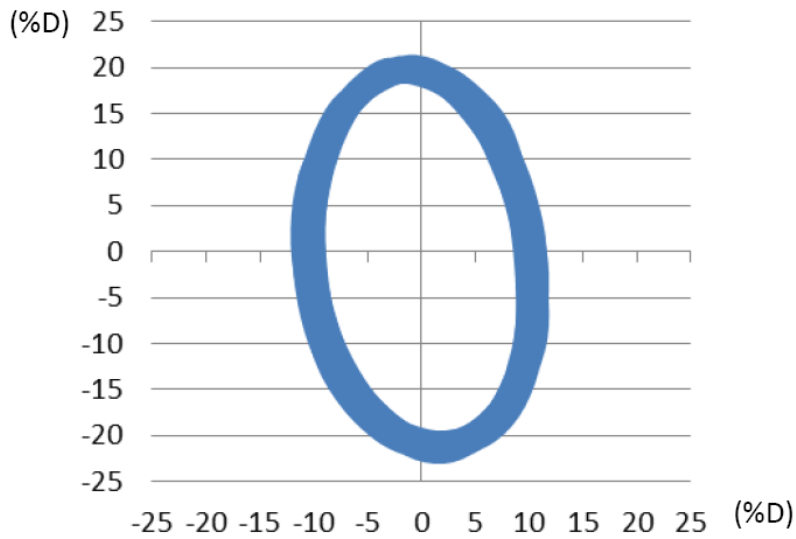


FIGURE 5. Orbiting responses of the cylinder at an inlet flow velocity 1.75 m/s. D is the diameter of the cylinder.

installed inside the cylinder at the middle of the span. They measured the strength of the cylinder vibrations and forwarded them to an industrial computer, which converted the signals to displacements. At a higher inlet flow velocity 1.75 m/s, the cylinder traced elliptical trajectories in the experiment (Figure 5). The elliptical trajectories implied that the streamwise and transverse orbiting responses had the same frequency but with a phase shift. Kheirkhah et al. [17] showed that for a range of flow velocities, referred as the synchronization region, the transverse and streamwise frequencies lock onto the natural frequency of the structure, and the cylinder traces elliptical trajectories. As illustrated in Figure 6, alternating strong vortices were created on the downstream side of the cylinder, and strong vortex shedding happened behind the cylinder because the vortex-shedding frequency matched the natural frequency of the cylinder.

Three learning classifiers, based on K-nearest neighbor (KNN) [18], artificial neural network (ANN) [19], and Bayes classifier (BC) [20] methods, were compared with the proposed method. Similarly, 80 data sets were randomly selected as training samples, and the other 200 sets were used as validation samples for evaluating the performance of the classifiers. In the KNN classification, the input data were a set of $\{C_4, C_5, C_6, C_7\}$, and the output was a class membership ($\{A\}, \{B\}, \{C\}, \{D\}$). The input images were classified by a majority vote of their $k = 5$ nearest neighbors. The ANN was a three-layer

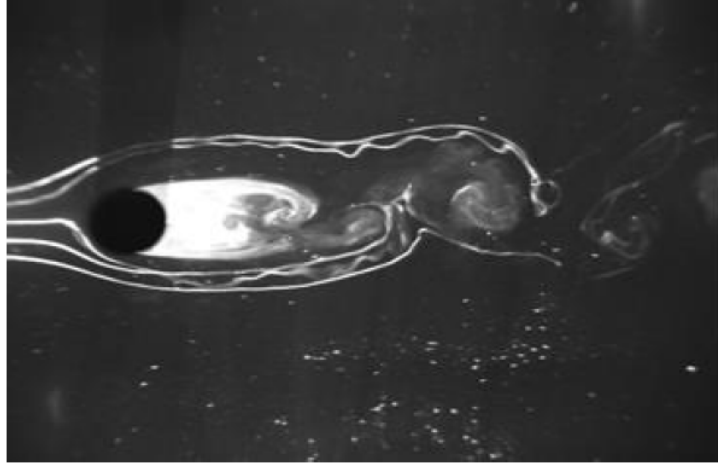


FIGURE 6. Wake patterns caused by cylinder vibrations at an inlet flow velocity 1.75 m/s

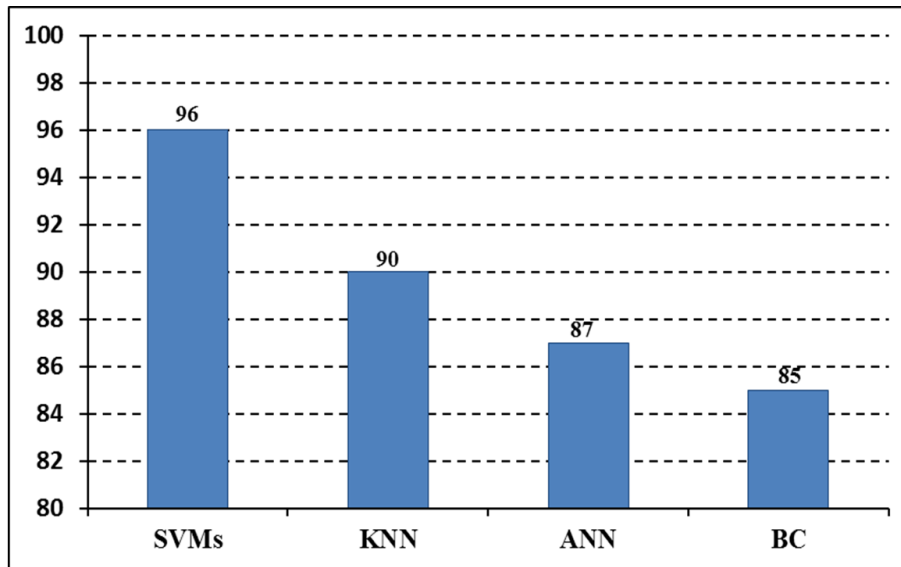


FIGURE 7. Comparison of the accuracy rates (%) from various classifiers

neural network with four neurons ($\{C_4, C_5, C_6, C_7\}$) in the input layer, six neurons in the hidden layer, and four neurons ($\{A\}, \{B\}, \{C\}, \{D\}$) in the output layer. The BC is given as follows:

$$D(x) = -\frac{1}{2} \ln |C_j| - \frac{1}{2} [(x - m_j)^T C_j^{-1} (x - m_j)] \quad (3)$$

where x was a set of $\{C_4, C_5, C_6, C_7\}$ derived from an input image. The mean vectors m_j and the covariance matrix C_j of the coefficients for the j class were derived. The input images were identified as the j class by minimizing the calculated value of $D(x)$. Figure 7 provides the experimental accuracy rates. The accuracy rates were 96% for the SVMs, 90% for the KNN, 87% for the ANN, and 85% for the BC, demonstrating that the SVMs classified images with the greatest accuracy. This may be because the SVMs mapped the input data sets into a high-dimensional feature space and maximized the margin between two classes in the feature space. The high-dimensional feature space is suitable even for cases with small sample sizes (e.g., small number of training samples).

Then, hybrid schemes of feature extraction methods combined with SVMs were compared to test the proposed method. The feature extraction methods combined with the SVMs for the EFD, discrete wavelet transform (DWT) [21], and moment invariants (INV) [22] were denoted as EFD-SVMs, DWT-SVMs, and INV-SVMs, respectively. For the DWT feature extraction, an image signal was decomposed into various scales at different levels of resolution. The relationships among the DWT coefficients were expressed as follows:

$$A_0 = A_j + \sum_{j=1}^i D_j \quad (4)$$

where A_j and D_j were approximation and detail coefficients at j -level decomposition, respectively. For the process of the decomposition, the initialization of A_0 was the original image signal and j was set to 6. For the INV feature extraction, a segmented image f with gray pixel values at pixel (x, y) was denoted as $f(x, y)$, and the central moment was expressed as

$$\mu_{pq} = \int_{-\infty}^{\infty} \int_{-\infty}^{\infty} (x - x_c)^p (y - y_c)^q f(x, y) dx dy \quad (5)$$

where (x_c, y_c) were the coordinates of the segmented image centroid. The seven Hu-type INVs derived from the central moments of the second or third order ($p + q = 2$ or 3), $[\phi_i]_{i=1,2,3,\dots,7}$, were used as features.

To evaluate the hybrid methods, the same block diagram (Figure 1) used in the proposed method was employed. (1) The 200 validation samples for each type were input from the image queue. (2) The input images were converted and passed to a feature-based algorithm (EFD, DWT, and INV). (3) SVMs classified images. (4) The image queue was checked for remaining images. A time-cost function $T(n)$ approximately quantified the amount of time required for an algorithm used in binary search tree operations, and it was described by

$$T(n) = O(\log n), \quad (6)$$

where $O(\log n)$ bounded the logarithmic time required by an algorithm for all n -sized inputs in the big-O notation, excluding coefficients and lower-order terms. Figure 8 presents

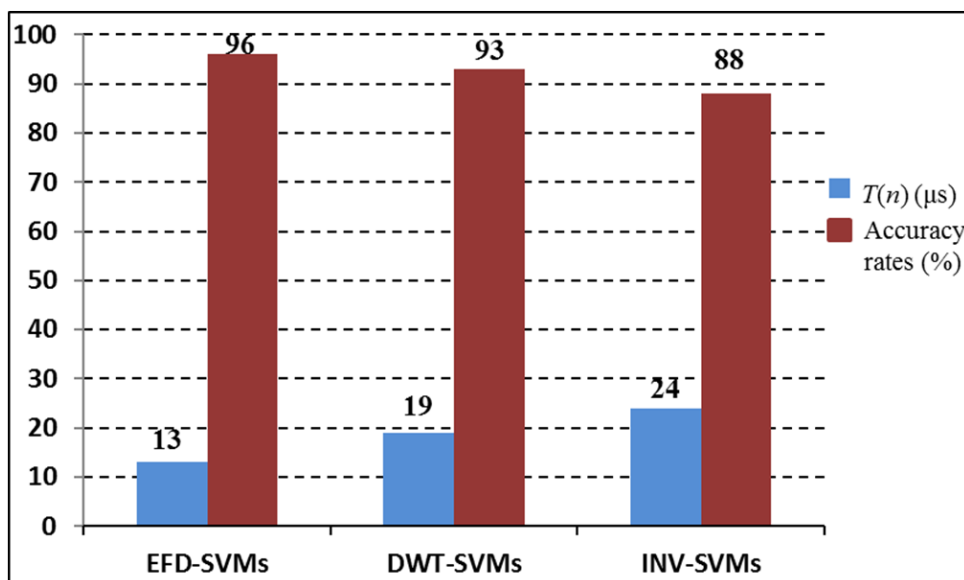


FIGURE 8. Time-cost function $T(n)$ and accuracy rates from hybrid methods in VIV detection

the time-cost function $T(n)$ and classification accuracy rates in VIV detection. The accuracy rates were 96% for the proposed algorithm, 93% for the DWT-SVMs method, and 88% for the INV-SVMs method. The time-cost function $T(n)$ for the proposed algorithm was lower than that in the other two methods because the hybrid EFD/SVM method could directly use the edge descriptors in the ARG segmented image to recognize the wake patterns. Therefore, the proposed algorithm outperformed the other hybrid methods.

5. Conclusions. This paper proposes a hybrid vision-based method for adaptively segmenting and effectively classifying object samples. The proposed method can detect the patterns caused by VIV. The proposed algorithm can employ suitable image parameters to inspect objects. The proposed algorithm can solve the VIV detection problem associated with concurrently measuring the whole flow field. The results demonstrate that the proposed algorithm can adaptively segment the sample images and determine continuous contours by using suitable descriptors. The detection system can sense image patterns and apply suitable image parameters to attaining an average recognition rate of 96%. The proposed method outperformed existing hybrid methods (DWT-SVMs and INV-SVMs). However, pattern detection in a multisensor system may be a challenge in computer vision. The data from multiple sensors include noise and irrelevant information; this impedes signal processing. Further research directions include creating a processing framework for establishing indicators and corresponding thresholds to detect patterns in the system.

Acknowledgment. This work was supported by Shih Chien University under Project 105-05-05002-03.

REFERENCES

- [1] F. J. Huera-Huarte, Z. A. Bangash and L. M. Gonzalez, Towing tank experiments on the vortex-induced vibrations of low mass ratio long flexible cylinders, *Journal of Fluids and Structures*, vol.48, pp.81-92, 2014.
- [2] Z. Feng, N. Jiang, F. Zang, Y. Zhang, X. Huang and W. Wu, Nonlinear characteristics analysis of vortex-induced vibration for a three-dimensional flexible tube, *Commun. Nonlinear Sci. Numer. Simulat.*, vol.34, pp.1-11, 2016.
- [3] H. Tang, P. Salunkhe, Y. Zheng, J. Du and Y. Wu, On the use of synthetic jet actuator arrays for active flow separation control, *Experimental Thermal and Fluid Science*, vol.57, pp.1-10, 2014.
- [4] C. Wang, H. Tang, F. Duan and S. C. M. Yu, Control of wakes and vortex-induced vibrations of a single circular cylinder using synthetic jets, *Journal of Fluids and Structures*, vol.60, pp.160-179, 2016.
- [5] H. Park, R. A. Kumar and M. M. Bernitsas, Suppression of vortex-induced vibrations of rigid circular cylinder on springs by localized surface roughness at $3 \times 10^4 \leq Re \leq 1.2 \times 10^5$, *Ocean Engineering*, vol.111, pp.218-233, 2016.
- [6] M. Yang and T. Su, Automated diagnosis of sewer pipe defects based on machine learning approaches, *Expert Systems with Applications*, vol.35, no.3, pp.1327-1337, 2008.
- [7] F. Serdio, E. Lughofer, K. Pichler, M. Pichler, T. Buchegger and H. Efendic, Fault detection in multi-sensor networks based on multivariate time-series models and orthogonal transformations, *Information Fusion*, vol.20, pp.272-291, 2014.
- [8] Z. L. Tseng, K. R. Aleti, Z. Hu and Y. Kwon, E-quality: A support vector machines approach, *Journal of Computational Design and Engineering*, vol.3, pp.91-101, 2016.
- [9] R. Guillermo, P. H. Emilio, A. R. Jorge and M. M. T. Juan, Multiple partial discharge source discrimination with multiclass support vector machines, *Expert Systems with Applications*, vol.55, pp.417-428, 2016.
- [10] R. M. Barbosa, E. S. Paula, A. C. Paulelli, A. F. Moore, J. M. O. Souza, B. L. Batista, A. D. Campiglia and F. Barbosa Jr., Recognition of organic rice samples based on trace elements and support vector machines, *Journal of Food Composition and Analysis*, vol.45, pp.95-100, 2016.

- [11] X. Liang, L. Zhu and D. S. Huang, Multi-task ranking SVM for image cosegmentation, *Neurocomputing*, vol.247, pp.126-136, 2017.
- [12] B. Yu, B. Jia, L. Ding, Z. Cai, Q. Wu, R. Law, J. Huang, L. Song and S. Fu, Hybrid dual-tree complex wavelet transform and support vector machine for digital multi-focus image fusion, *Neurocomputing*, vol.182, pp.1-9, 2016.
- [13] M. A. Ebrahimi, M. H. Khoshtaghaza, S. Minaei and B. Jamshidi, Vision-based pest detection based on SVM classification method, *Computers and Electronics in Agriculture*, vol.137, pp.52-58, 2017.
- [14] K. Lekdioui, R. Messoussi, Y. Ruichek, Y. Chaabi and R. Touahni, Facial decomposition for expression recognition using texture/shape descriptors and SVM classifier, *Signal Processing: Image Communication*, vol.58, pp.300-312, 2017.
- [15] T.-K. Lin, A novel automated inspection approach based on adaptive region-growing image segmentation, *Journal of the Chinese Society of Mechanical Engineers*, vol.35, no.1, pp.57-65, 2014.
- [16] T.-K. Lin, Adaptive learning method for multiple-object detection in manufacturing, *Advances in Mechanical Engineering*, vol.7, no.12, pp.1-12, 2015.
- [17] S. Kheirkhah, S. Yarusevych and S. Narasimhan, Orbiting response in vortex-induced vibrations of a two-degree-of-freedom pivoted cylinder, *Journal of Fluids and Structures*, vol.28, pp.343-358, 2012.
- [18] M. Du, S. Ding and H. Jia, Study on density peaks clustering based on k-nearest neighbors and principal component analysis, *Knowledge-Based Systems*, vol.99, pp.135-145, 2016.
- [19] M. Moghadam and S. Asgharzadeh, On the application of artificial neural network for modeling liquid-liquid equilibrium, *Journal of Molecular Liquids*, vol.220, pp.339-345, 2016.
- [20] R. O. Mujalli, G. Lopez and L. Garach, Bayes classifiers for imbalanced traffic accidents datasets, *Accident Analysis and Prevention*, vol.88, pp.37-51, 2016.
- [21] K. Pattanaworapan, K. Chamnongthai and J. M. Guo, Signer-independence finger alphabet recognition using discrete wavelet transform and area level run lengths, *Journal of Visual Communication and Image Representation*, vol.38, pp.658-677, 2016.
- [22] J. Kautsky and J. Flusser, Numerical problems with Pascal triangle in moment computation, *Journal of Computational and Applied Mathematics*, vol.306, pp.53-68, 2016.